Modeling of the Solidification Process in a Continuous Casting Installation for Steel Slabs

MARCIAL GONZALEZ, MARCELA B. GOLDSCHMIT, ANDREA P. ASSANELLI, ELENA FERNÁNDEZ BERDAGUER, and EDUARDO N. DVORKIN

The development of a computational simulation system for modeling the solidification process in a continuous casting facility for steel slabs is discussed. The system couples a module for solving the direct problem (the calculation of temperatures in the steel strand) with an inverse analysis module that was developed for evaluating the steel/mold heat fluxes from the information provided by thermocouples installed in the continuous casting mold copper plates. In order to cope with the non-uniqueness of the inverse analysis, *a priori* information on the solution, based on the consideration of the problem physics, is incorporated. The stability of the system predictions are analyzed and the influence of the first trial used to start the evaluation procedure is discussed. An industrial case is analyzed.

I. INTRODUCTION

NOWADAYS almost 90 pct of the world steel production is being produced in continuous casting installations;[1] therefore, this is a technology with a very important economical impact. The continuous casting technology, which was originated almost 50 years ago and which in 1970 attained only 4 pct of the world steel production,[1] is still undergoing important developments due to the fact that the requirements on the product quality and on the production efficiency are continuously being increased. These developments incorporate not only equipment revamps but also updates in the installation setups and in their process controls.

The first requirement to develop a successful setup and a tight control of any process is to have an in-depth knowledge of the process *technological windows*, that is to say, of the locus in the space of the process control variables, where the products meet the required specifications.[2,3]

Computational models are nowadays a powerful and reliable tool to simulate different thermomechanical-metallurgical processes; hence, they are increasingly being used to investigate the technological windows of different processes in the steel industry, such as continuous casting, hot rolling, cold rolling, heat treatments, etc.[4]

A schematic representation of a continuous casting installation for steel slabs in shown in Figure 1, where we can identify the following process sequence:

(1) The liquid steel is poured into a copper mold, which is refrigerated with an external water jacket. The cooling of the steel and its solidification inside the mold progress from the outside to the inside; therefore, the external solidified steel shell increases its thickness as the steel strand transits the mold.

The physical process inside the mold is quite complex because the solidified steel shell and the mold are strained due to thermal and mechanical loads (ferrostatic pressure). While at the meniscus the steel is in contact with the mold intrados, downstream, a gap is opened between the strand and the mold. However, in some cases, the mold is shaped so as to regain its contact with the strand at its lower sections.[5]

Usually, the slab molds are equipped with thermocouples located through the thickness of its copper piates; the indications of these thermocouples are the input to a heuristic algorithm that provides break-out alarms.

The mathematical description of the heat transfer between the strand and the mold requires a model that couples the heat-transfer equations with the description of the mold thermomechanical deformations.[6]

An alternative procedure is to use an empirical law that describes the heat flow between the steel strand and the mold, *e.g.*, the Savage–Pritchard[7] equation and its modifications proposed by Brimacombe and Weinberg.[8] As it is well known, this approach may introduce important deviations between the model predictions and the actual temperature distribution.

Another alternative we develop in the present article is to use the indications of the mold thermocouples to evaluate, *via* an inverse analysis procedure, the heat-transfer coefficients that govern the thermal process in the mold; in this way, an uncoupled heat-transfer analysis can be performed.

(2) The steel strand exits the mold and continues its solidification. The distance, measured along the slab centerline, between the meniscus and the section at which the strand solidification is completed is called the *metallurgical length*.

After existing the mold, the steel strand is cooled with water jets and also by interchanging heat with refrigerated guide rolls.

MARCIAL GONZALEZ, Research Engineer, MARCELA B. GOLDSCHMIT, Head, Computational Mechanics Department, ANDREA P. ASSANELLI, Head, Full Scale Testing Laboratory, and EDUARDO N. DVORKIN, General Director, are with the Center for Industrial Research, FUDETEC Av. Córdoba 320 1054, Buenos Aires, Argentina. Contact e-mail: dvk@siderca.com ELENA FERNÁNDEZ BERDAGUER, Professor, is with CONICET, Instituto de Calculo, Science School, University of Buenos Aires, Ciudad Universitaria–Pabellón 2, Buenos Aires, Argentina.

Manuscript submitted July 24, 2002.

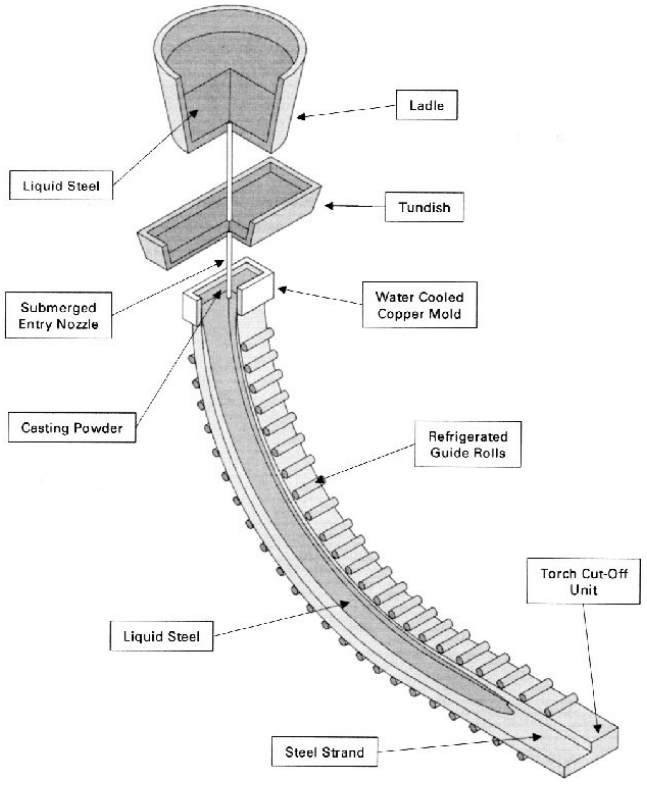

Fig. 1—Scheme of a continuous casting installation for steel slabs.

In a continuous casting installation, in order to gain productivity, the strand extraction velocity has to be increased as much as possible; however, this means that

(1) the metallurgical length increases,
(2) the stresses acting on the solidified shell become larger, and
(3) bulging between cylinders becomes more critical due to the smaller thickness of the solidified shell.

Of course, the aforementioned phenomena depend on the chemical composition of the steel being casted. To be able to quantify those phenomena, a thermomechanical-metallurgical model of the continuous casting process is required.

The computational system that we developed, CCAST, is composed of two coupled modules: CCAST-D and CCAST-I.

In the second section of this article, we discuss the robust numerical algorithm that we implemented in the finite element code CCAST-D, to solve the direct problem for the cooling of a steel strand; this model incorporates the description of phase transformation phenomena: from the liquid phase to the solid phase and also solid phase transformations.

In the third section of this article, we present the inverse analysis methodology developed to identify the heat-transfer coefficients that we use to model the steel strand solidification inside the mold. This inverse analysis was implemented in the module CCAST-I.

In the fourth section of this article, we discuss a set of numerical examples: the first one is a parametric analysis of a slab's continuous casting facility; in this example, we investigate using CCAST-D the effect of the different operational parameters on the casted slabs temperature map and on their metallurgical length. In the second example, we investigate the stability of the CCAST predictions when the input values are perturbed. In the third example, we discuss the effect of the *initial guess* on the output of the inverse analysis, and finally, in the fourth example, we present an actual industrial application.

II. AN ALGORITHM FOR MODELING HEAT-TRANSFER PROBLEMS INCLUDING PHASE TRANSFORMATIONS

The numerical modeling of heat-transfer problems including phase transformation phenomena has been the subject of much research; among others, we refer to the works of Morgan *et al.*,[9] Rolph and Bathe,[10] Tamma and Namburu,[11] Song *et al.*,[12] Swaminathan and Voller,[13] Crivelli and Idelsohn,[14] Storti *et al.*,[15] and Fachinotti *et al.*[16]

Based on those previous research efforts, we implemented a formulation for modeling the thermal process in the continuous casting of steel; this formulation incorporates two phase changes: liquid to solid and a solid-state phase transformation (phase δ to γ and γ to α).

In the implemented formulation, we start from the heat balance equation:

$$\frac{\partial \mathcal{H}}{\partial t} - \underline{\nabla} \cdot (k \, \underline{\nabla} T) = q_V \qquad [1]$$

where

$\mathcal{H}$ = enthalpy per unit volume of the reference configuration,
k = coefficient of heat conduction,
T = temperature, and
q_V = heat generated per unit volume of the reference configuration.

For a phase change in steel, either from liquid to solid or inside the solid phase, the temperature is not constant as in pure substances such as water. In Figure 2,[10] we represent a typical curve $\mathcal{H} = \mathcal{H}(T)$, where L is the latent heat per unit mass and ρ is the density.

For low alloy steels of different chemical compositions, we obtain the curves $\mathcal{H} = \mathcal{H}(T)$ from Reference 17. In Figure 3, we show the corresponding curves of enthalpy, per unit mass, for a typical low carbon steel and for a peritectic steel.

Taking into account the dependence $\mathcal{H} = \mathcal{H}(T)$, we can write Eq. [1] as

$$\frac{d\mathcal{H}}{dT}\frac{\partial T}{\partial t} - \underline{\nabla} \cdot (k \, \underline{\nabla} T) = q_V \qquad [2]$$

We can also calculate

$$\frac{d\mathcal{H}}{dT} = \rho_s \, \bar{c}_s \ (\text{for } T \le T_s) \qquad [3a]$$

$$\frac{d\mathcal{H}}{dT} = (\mathcal{H}_l - \mathcal{H}_s)/(T_l - T_s) \quad (\text{for } T_s < T < T_l) \qquad [3b]$$

$$\frac{d\mathcal{H}}{dT} = \rho_l \, \bar{c}_l \ (\text{for } T \ge T_l) \qquad [3c]$$

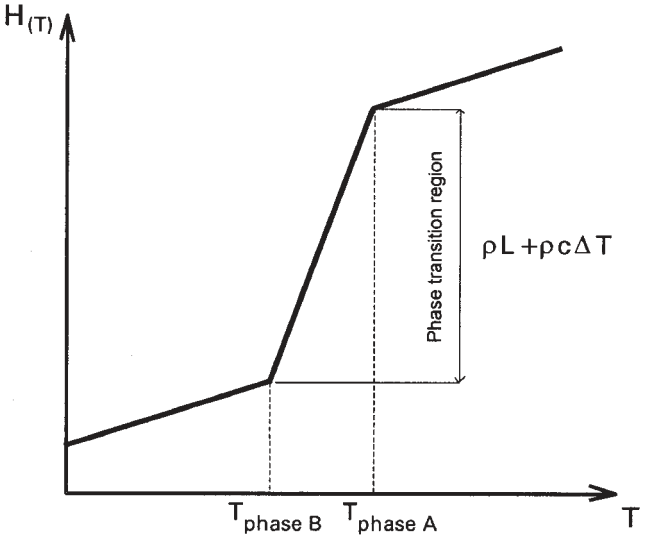

Fig. 2—Enthalpy as a function of temperature for a typical steel.

Please notice the following:

(1) Equation [3a] is valid for $T \leq T_s$, where T_s is the *solidus* temperature. In this equation, ρ_s is the solid density and $\bar{c}_s$ is the solid specific heat per unit mass (we assume it constant). Notice that the solid properties may correspond to the γ or α phase or to a state where we have a phase transformation; in this case, a formula similar to Eq. [3b] is used.
(2) Equation [3b] is valid for $T_s < T < T_l$, where T_l is the liquidus temperature. In this equation, $\mathcal{H}_l$ and $\mathcal{H}_s$ are the enthalpies per unit volume at the *liquidus* and *solidus* lines, respectively (we assume $d\mathcal{H}/dT$ to be constant inside the mushy zone).
(3) Equation [3c] is valid for $T \geq T_l$. In this equation, ρ_l is the liquid density and $\bar{c}_l$ is the liquid specific heat per unit mass (we assume it to be constant).

In order to simulate the effect of the convective heat transfer inside the liquid pool, we consider a majorated coefficient of heat conduction inside it[8] (on the basis of our numerical experimentation, we use $k = 8\ k_{\text{steel}}$).

For solving Eq. [2] in the continuous casted strand, we formulate a transient two-dimensional (2-D) finite-element model in which a rectangular cross section moves through the continuous caster exchanging heat first with the mold walls and afterward with the secondary cooling system (Figure 1). For developing this 2-D model as it is usually done, the heat transfer in the longitudinal direction is neglected. The cross section is discretized using four-node temperature-interpolated elements.[18]

We use the implicit *Euler-backward* method[18] to integrate the transient system of ordinary differential equations obtained *via* the Galerkin weighted residuals scheme. For solving the step from time t to time $t + \Delta t$, we get for the case $q_V = 0$

$$\left[{}^{t+\Delta t}\underline{C} + ({}^{t+\Delta t}\underline{K_k} + {}^{t+\Delta t}\underline{K_c})\right]{}^{t+\Delta t}\underline{T} = {}^{t+\Delta t}\underline{F_c} + {}^{t+\Delta t}\underline{F_q} + {}^{t+\Delta t}\underline{C}\,{}^{t}\underline{T} \qquad [4]$$

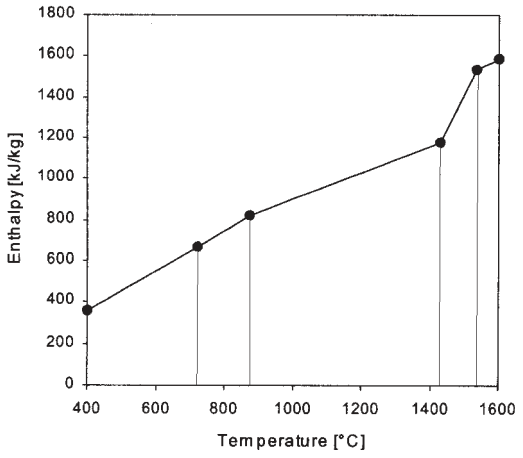

(a) Low carbon steel.

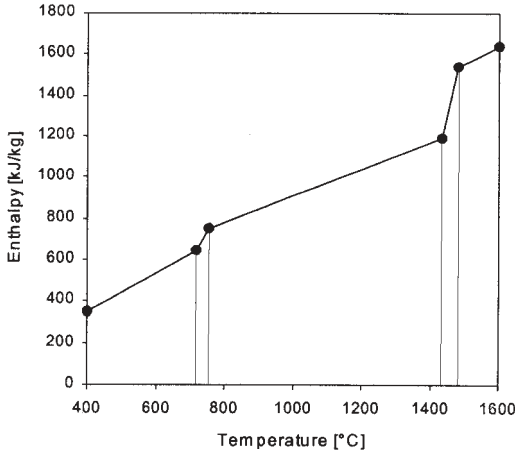

(b) Peritectic steel.

Notice the following in the preceding equation:

(1) The vectors ${}^{t+\Delta t}\underline{T}$ (unknown for the step) and ${}^{t}\underline{T}$ (data for the step) contain the nodal temperatures at times $t + \Delta t$ and t, respectively.
(2) The matrix ${}^{t+\Delta t}\underline{C}$ is the heat capacity matrix. Applying consistently the Galerkin weighted residual method, and considering $d\mathcal{H}/dt$ to be constant inside each element, we obtain for an element e

$${}^{t+\Delta t}\underline{C}^{(e)} = \frac{1}{\Delta t}\int_{V^{(e)}} {}^{t+\Delta t}\left[\frac{d\mathcal{H}}{dT}\right]_O \underline{H}^T\,\underline{H}\,dv \qquad [5]$$

In Eq. [5], the symbol $[\cdot]_O$ indicates that the term between brackets is calculated at the element center; and $\underline{H}$ is the temperature interpolation matrix inside the 2-D element.[18] Following what has been previously discussed in the literature, we use, instead of

the matrix in Eq. [5], the corresponding lumped capacity matrix, which for the four-node element of unit thickness is

$$ {}^{t+\Delta t}\underline{C}^{(e)} = \frac{1}{\Delta t_{\,t+\Delta t}} \left[\frac{\Delta \mathcal{H}}{\Delta T} \right]_O A_{(e)} \begin{bmatrix} \frac{1}{4} & 0 & 0 & 0 \\ 0 & \frac{1}{4} & 0 & 0 \\ 0 & 0 & \frac{1}{4} & 0 \\ 0 & 0 & 0 & \frac{1}{4} \end{bmatrix} \quad [6] $$

In Eq. [6], $A_{(e)}$ is the 2-D element area.

(3) The matrix ${}^{t+\Delta t}\underline{K_k}$ is the conduction matrix. Applying consistently the Galerkin weighted residual method, we obtain for an element e

$$ {}^{t+\Delta t}\underline{K_k}^{(e)} = \int_{V^{(e)}} \underline{B}^T \left[{}^{t+\Delta t}k \right]_O \underline{B} \, dv \quad [7] $$

In Eq. [7]

$$ {}_t\left[\frac{\partial T}{\partial x_i} \right] = \underline{B} \, {}^t\underline{T} \quad [8] $$

(4) When on a surface SC with external normal $\underline{n}$ we prescribe boundary conditions of the form ${}^{t+\Delta t}\underline{q_n} = {}^{t+\Delta th}({}^{t+\Delta t}T_s - {}^{t+\Delta t}T_{\text{environment}})$, we have to calculate the matrix

$$ {}^{t+\Delta t}\underline{K_c}^{(e)} = \int_{SC^{(e)}} \underline{H_S^T} \, \underline{H_S} \, {}^{t+\Delta th} \, dS \quad [9] $$

where $\underline{H_S}$ is the interpolation matrix particularized for the surface SC.

(5) The load vector ${}^{t+\Delta t}\underline{F_c}$ also comes from the boundary conditions discussed in the previous item:

$$ {}^{t+\Delta t}\underline{F_c}^{(e)} = \int_{SC^{(e)}} \underline{H_S^T} \, {}^{t+\Delta t}h \, {}^{t+\Delta t}T_{\text{environment}} \, dS \quad [10] $$

(6) The load vector ${}^{t+\Delta t}\underline{F_q}$ incorporates the heat flow that is prescribed on a surface SQ (*e.g.*, the heat flow imposed on the strand inside the mold):

$$ {}^{t+\Delta t}\underline{F_q}^{(e)} = -\int_{SQ^{(e)}} \underline{H_S^T} \, {}^{t+\Delta tqn} \, dS \quad [11] $$

where ${}^{t+\Delta tqn}$ is the imposed heat flux.

Equation [4] is nonlinear; therefore, it is necessary to solve them using an iterative technique. For the ith iteration, the equations are

$$ \left[{}^{t+\Delta t}\underline{C} + {}^{t+\Delta t}\underline{K_k} + {}^{t+\Delta t}\underline{K_c} \right]^{(i-1)} \Delta \underline{T}^{(i)} = {}^{t+\Delta t}\underline{F_c} + {}^{t+\Delta t}\underline{F_q} + {}^{t+\Delta t}\underline{C}^{(i-1)} \, {}^{t}\underline{T}^{(i-1)} - \left[{}^{t+\Delta t}\underline{C} + {}^{t+\Delta t}\underline{K_k} + {}^{t+\Delta t}\underline{K_c} \right]^{(i-1)} {}^{t+\Delta t}\underline{T}^{(i-1)} \quad [12a] $$

$$ {}^{t+\Delta t}T^{(i)} = {}^{t+\Delta t}\underline{T}^{(i-1)} + \Delta \underline{T}^{(i)} \quad [12b] $$

The preceding iterative scheme is complemented using a line search algorithm.[18,19]

The iterative procedure is continued until $\| \Delta \underline{T}^{(i)} \|_2 \leq$ *TTOL* (tolerance prescribed by the analyst).

III. THE STEEL SLABS CONTINUOUS CASTING THERMAL MODEL

The accurate description of the heat flow between the solidifying steel strand and the mold plates is fundamental information for the development of the thermal model of a continuous casting process, for the evaluation of different casting powders and, in general, for the evaluation of the process performance under different operational parameters and for different steel chemical compositions.

The law of Savage–Pritchard,[7] which is often used for modeling the heat flow between the steel strand and the mold in the continuous casting of slabs, can only be considered a qualitative approach and does not incorporate enough information for analyzing the effect of different steel chemical compositions or different casting powders, unless an experimental parameters determination is performed.

The *exact* modeling of the heat flow between the steel and the mold requires the prediction of the gap or contact pressure between them; hence, it requires the solution of a coupled thermomechanical problem.[6] This route is intellectually very rewarding because it is *self-contained* and it does not require the input of *field data*; however, it is not a practical engineering approach because it is numerically quite involved and convergence may not be achieved.

In this section, we present an inverse analysis procedure to evaluate the steel/mold heat flow using the output of the thermocouples installed inside the mold copper plates, as shown in Figure 4.

For the heat flow evaluation, we iteratively couple the inverse analysis module CCAST-I with the direct analysis module CCAST-D. The calculation in the CCAST system proceeds as shown in Figure 5 (*external loop*).

A. *The Copper Mold Temperature Model*

In Figure 6, we show the finite-element meshes that we used to analyze the four copper plates of the slab's continuous casting mold. In this figure, we also indicate the position of the available thermocouples.

For modeling the temperature distribution inside each copper plate, we consider

(1) steady-state heat exchange regime,
(2) constant thermal conductivity coefficient ($k_{\text{mold}} = 350 \, \frac{W}{mK}$),
(3) no heat flux between copper plates, and
(4) convective heat exchange between the mold copper plates and the water in the cooling channels,[20]

$$ q_{\text{water}} = h_{\text{water}}(T_{\text{mold}} - T_{\text{water}}) \quad [13a] $$

$$ \frac{h_{\text{water}} \, D_h}{k_{\text{water}}} = 0.023 \left(\frac{\rho_{\text{water}} \, \bar{v}_{\text{water}} \, D_h}{\mu_{\text{water}}} \right)^{0.8} \left(\frac{cp_{\text{water}} \, \mu_{\text{water}}}{k_{\text{water}}} \right)^{0.4} \quad [13b] $$

$$ D_h = \frac{4 \text{ Transverse area of water channels}}{\text{Perimeter of water channels}} \quad [13c] $$

$$ cp_{\text{water}} = 4181 \, \frac{\text{J}}{\text{kg K}} \text{ (water specific heat)} \quad [13d] $$

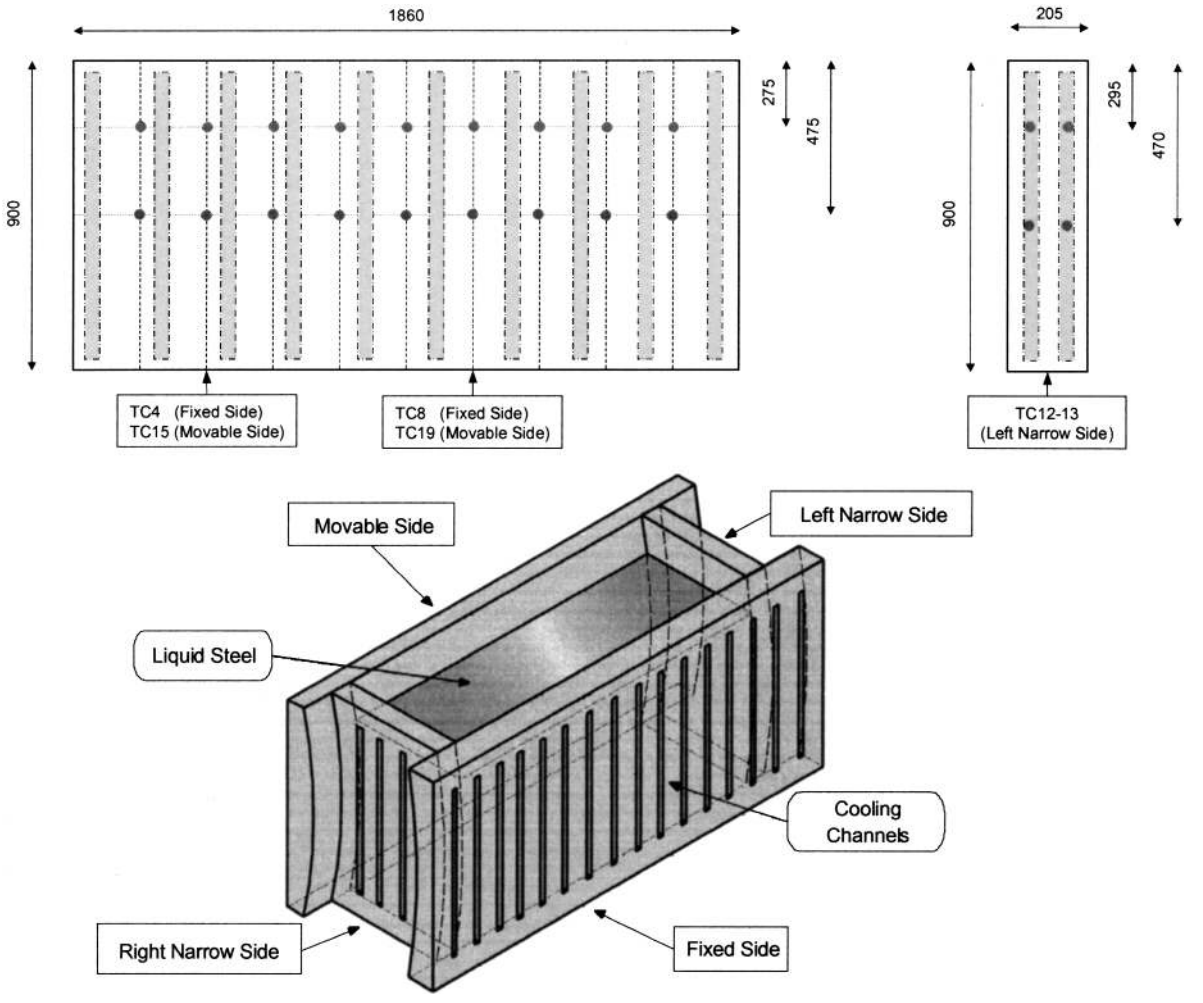

Fig. 4—Thermocouples installed in the mold of a steel slab's continuous casting installation.

$$k_{water} = 0.602 \frac{W}{mK} \text{ (water thermal conductivity)} \quad [13e]$$

$$\rho_{water} = 998 \frac{kg}{m^3} \text{ (water density)} \quad [13f]$$

$$\mu_{water} = 0.000968 \frac{kg}{ms} \text{ (water viscosity)} \quad [13g]$$

T_{water}: cooling water temperature, a linear variation from the inlet to the outlet is assumed [13h]

T_{mold}: temperature distribution in the mold areas in contact with the cooling water [13i]

$$\bar{v}_{water} = 7 \frac{m}{s} \text{ average water velocity} \quad [13j]$$

(5) A heat flux between the steel shell and the mold,

$$q_{steel/mold} = h_{steel/mold} (T_{mold} - T_{steel}) \quad [14]$$

in Eq. [14], $h_{steel/mold}$, is the heat-transfer coefficient to be evaluated using the inverse analysis procedure; this coefficient is a function of the position on the mold plate surfaces. T_{steel}: the temperature on the steel shell surface, function of the position on that surface. T_{mold}: the temperature on the considered mold plate inner surface, function of the position on this surface.

(6) Radiative heat exchange between the mold walls above the free casting powder surface, this surface, and the atmosphere (we use a radiation shape factor of 0.45 for these surfaces[20]).

(7) The remaining surfaces are assumed adiabatic.

B. *Inverse Analysis*

The field data for each copper plate are as follows.

(1) The thermocouple measurements in the mold plates, T_i^M, for $i = 1$ to Nth, where Nth is the number of thermocouples installed in each plate under analysis.

(2) The energy extracted by the plate cooling water (Q_w^M) is

$$Q_w^M = G_{water}^M \rho_{water} cp_{water} \Delta T_{water}^M \quad [15]$$

where

G_{water}^M = measured water flow rate, and
ΔT_{water}^M = measured water temperature increment.

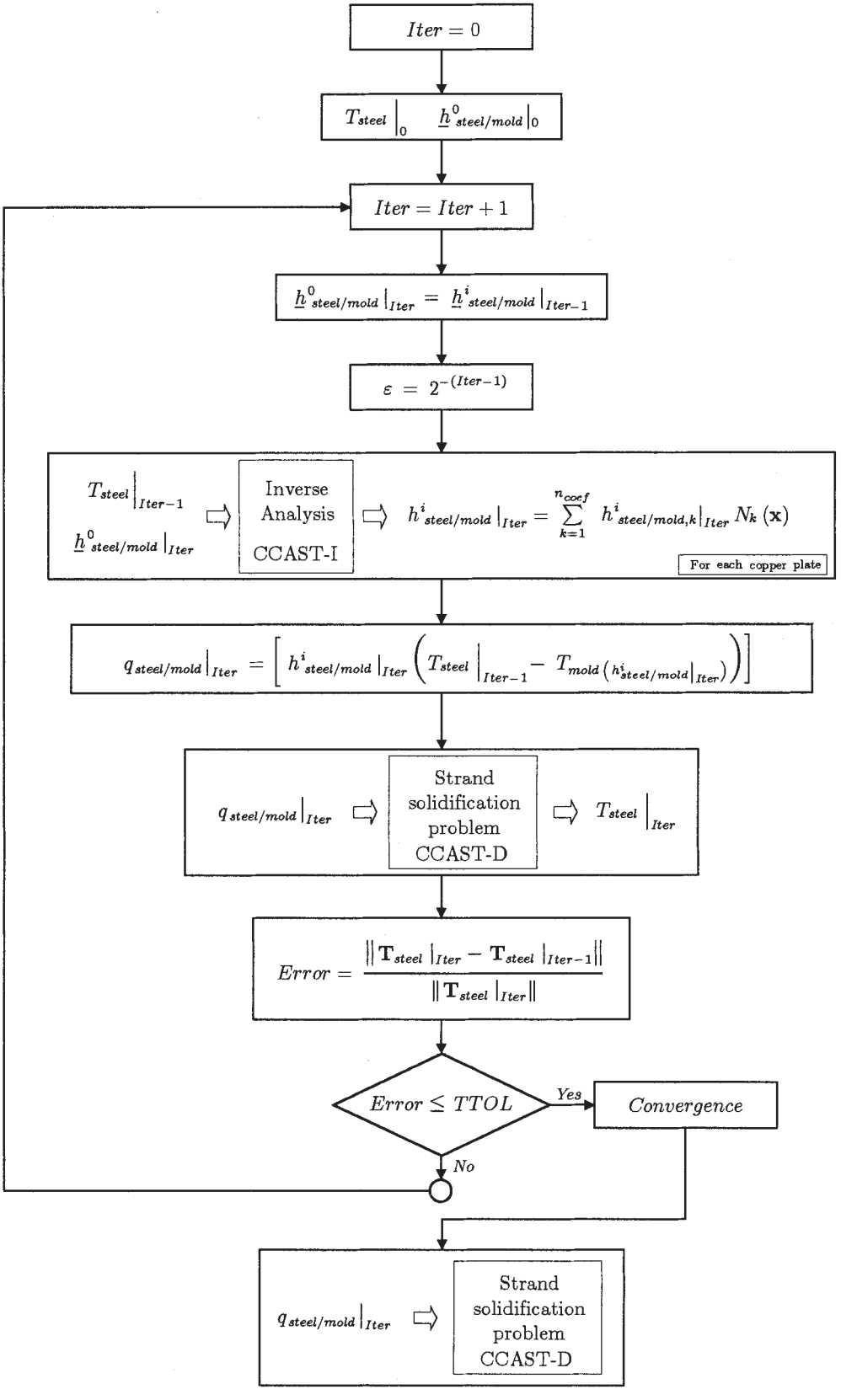

Fig. 5—Iterative loop between the inverse analysis module (CCAST-I) and the direct thermal solver (CCAST-D) (external loop).

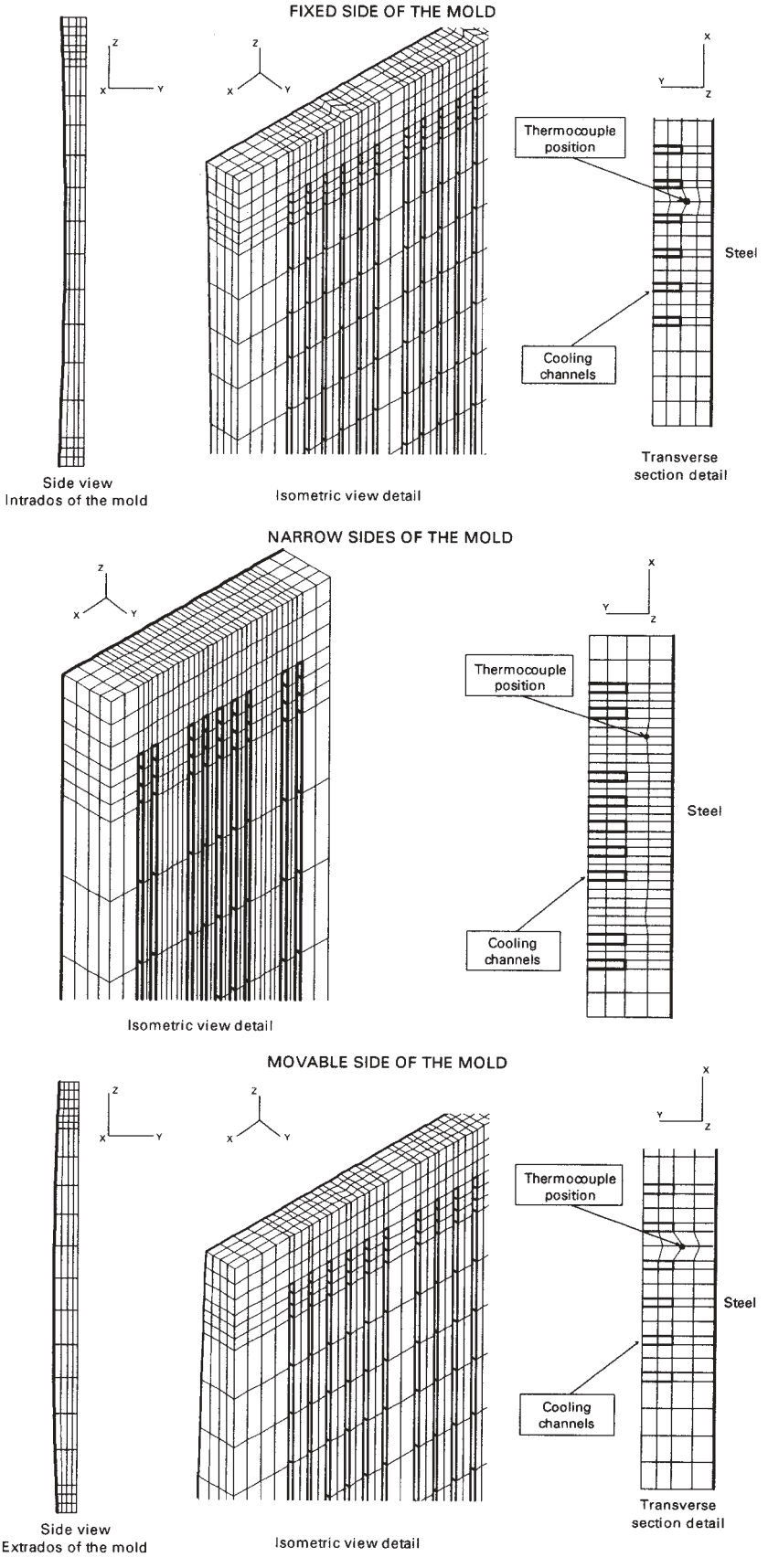

Fig. 6—Finite-element meshes used to analyze the copper mold plates.

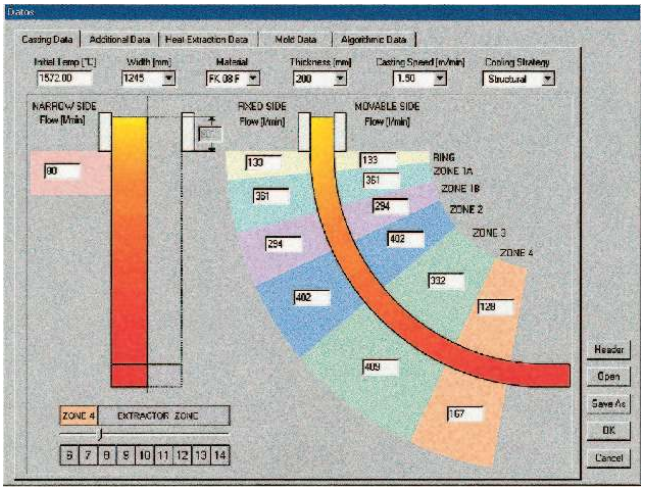

Fig. 7—Water cooling zones.

For each of the four plates, we assume a discretized heat-transfer coefficient function:

$$h_{\text{steel/mold}} = \sum_{k=1}^{N_{\text{coef}}} N_k h_{\text{steel/mold},k} \qquad [16]$$

where the functions N_k are piecewise constant interpolation functions. We seek the set of values $h_{\text{steel/mold},k}$ (k = 1 to N_{coef}) that satisfies the conditions

$$T_i^M - T_i^{\text{FEM}} = 0 \quad i = 1 \text{ to } N\text{th} \qquad [17a]$$

$$Q_w^M - Q_w^{\text{FEM}} = 0 \qquad [17b]$$

In the above equations, $(\cdot)^{\text{FEM}}$ is the value of $(\cdot)$ determined using the finite-element model.

The evaluation of the heat-transfer coefficients proceeds as follows:

(1) We start the inverse analysis assuming a set $h^{(0)}_{\text{steel/mold},k}$ (k = 1 to N_{coef}) (*initial guess*), or in case the external loop has already started, we use as initial set, the values obtained from the previous external iteration (Figure 5).
(2) We use the preceding coefficients, together with the corresponding slab surface temperature distribution calculated using CCAST-D, to calculate the values of ${}^{(0)}T_i^{\text{FEM}}$ and ${}^{(0)}Q_w^{\text{FEM}}$ using the mold plate model; normally, these values will not satisfy the conditions in Eqs. [17a] and [17b].
(3) $k = 0$ (start the iterative procedure)
(4) $k = k + 1$
(5) We can write using the first term of a Taylor's expansion,

$${}^{(k)}T_i^{\text{FEM}} = {}^{(k-1)}T_i^{\text{FEM}} + \sum_{j=1}^{N_{\text{coef}}} \left.\frac{\partial T_i^{\text{FEM}}}{\partial h_{\text{steel/mold},j}}\right|_{\underline{h}^{(k-1)}_{\text{steel/mold}}} \left(h^{(k)}_{\text{steel/mold},j} - h^{(k-1)}_{\text{steel/mold},j}\right) \quad i = 1 \ldots N\text{th} \qquad [18a]$$

$${}^{(k)}Q_w^{\text{FEM}} = {}^{(k-1)}Q_w^{\text{FEM}} + \sum_{j=1}^{N_{\text{coef}}} \left.\frac{\partial Q_w^{\text{FEM}}}{\partial h_{\text{steel/mold},j}}\right|_{\underline{h}^{(k-1)}_{\text{steel/mold}}} \left(h^{(k)}_{\text{steel/mold},j} - h^{(k-1)}_{\text{steel/mold},j}\right) \qquad [18b]$$

Cooling Zone	Cooling Water Profile
Pulverization Ring	Constant for standard widths.
Zone IA	Constant for standard widths.
Zona IB	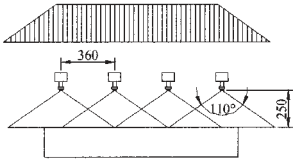
Narrow Zone	Constant for standard thicknesses.
Zone II (Segments 1-2)	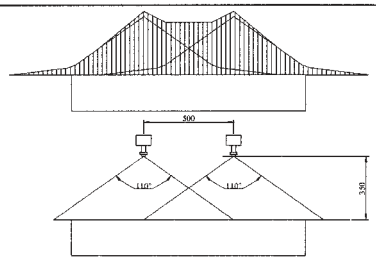
Zone III (Segments 3-5)	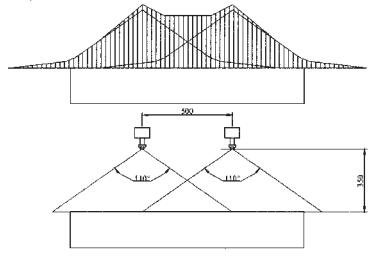
Zone IV (Segments 6-7)	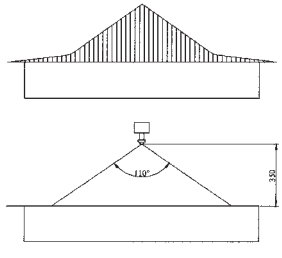

Fig. 8—Water jet arrangement in each cooling zone.

(6) Replacing Eqs. [18a] and [18b] in Eqs. [17a] and [17b], we get the following system of linear equations:

$$\sum_{j=1}^{N_{\text{coef}}} \left.\frac{\partial T_i^{\text{FEM}}}{\partial h_{\text{steel/mold},j}}\right|_{\underline{h}^{(k-1)}_{\text{steel/mold}}} \left(h^{(k)}_{\text{steel/mold},j} - h^{(k-1)}_{\text{steel/mold},j}\right) = T_i^M - {}^{(k-1)}T_i^{\text{FEM}} \quad i = 1 \ldots N\text{th} \qquad [19a]$$

$$\sum_{j=1}^{N_{\text{coef}}} \left.\frac{\partial Q_w^{\text{FEM}}}{\partial h_{\text{steel/mold},j}}\right|_{\underline{h}^{(k-1)}_{\text{steel/mold}}} \left(h^{(k)}_{\text{steel/mold},j} - h^{(k-1)}_{\text{steel/mold},j}\right) = Q_w^M - {}^{(k-1)}Q_w^{\text{FEM}} \qquad [19b]$$

The preceding equation system can be written as

$$\underline{A}\,\underline{x} = \underline{b} \qquad [20]$$

Table I. Data for the Analyzed Cases*

Case	*Th* (mm)	*w* (mm)	*v* (m/min)	T_w (°C)	T_e (°C)	ε	α
Base	200	1000	1.4	30	80	0.8	4.0
1	200	700	1.4	30	80	0.8	4.0
2	200	1300	1.4	30	80	0.8	4.0
3	200	1600	1.4	30	80	0.8	4.0
4	180	1000	1.4	30	80	0.8	4.0
5	200	1000	1.2	30	80	0.8	4.0
6	200	1000	1.6	30	80	0.8	4.0
7	200	1000	1.4	25	80	0.8	4.0
8	200	1000	1.4	30	60	0.8	4.0
9	200	1000	1.4	30	80	0.8	3.0
10	200	1000	1.4	30	80	0.8	5.0
11	200	1000	1.4	30	80	0.9	4.0

**Th*: slab thickness; and *w*: slab width. The analyses provided the results listed in Table II.

Table II. Analysis Results*

Case	L_{met} (mm)	Ts_{max} (°C)	*Dlm* (mm)
0	17,352	950	−144
1	17,337	950	986
2	17,354	950	−625
3	17,354	950	−1189
4	14,584	941	−28
5	14,656	912	9
6	20,333	982	−232
7	17,058	942	−137
8	17,350	950	−143
9	15,823	908	−71
10	18,593	982	−145
11	17,148	944	−124

*L_{met}: metallurgical length measured along the strand axis; Ts_{max}: temperature peak, on the slab upper face central line, after exiting the water cooling zone; and *Dlm*: a measure of the nonflatness of the solidification front zone defined in Fig. 9.

where

$$\underline{x} = \underline{h}^{(k)}_{\text{steel/mold}} - \underline{h}^{(k-1)}_{\text{steel/mold}} \quad [21]$$

$$\underline{A} = \begin{bmatrix} \left.\frac{\partial T_1^{\text{FEM}}}{\partial h_{\text{steel/mold},1}}\right|_{\underline{h}^{(k-1)}_{\text{steel/mold}}} & \cdots & \left.\frac{\partial T_1^{\text{FEM}}}{\partial h_{\text{steel/mold},N_{\text{coef}}}}\right|_{\underline{h}^{(k-1)}_{\text{steel/mold}}} \\ \cdots & \cdots & \cdots \\ \left.\frac{\partial T_{N\text{th}}^{\text{FEM}}}{\partial h_{\text{steel/mold},1}}\right|_{\underline{h}^{(k-1)}_{\text{steel/mold}}} & \cdots & \left.\frac{\partial T_{N\text{th}}^{\text{FEM}}}{\partial h_{\text{steel/mold},N_{\text{coef}}}}\right|_{\underline{h}^{(k-1)}_{\text{steel/mold}}} \\ \left.\frac{\partial Q_w^{\text{FEM}}}{\partial h_{\text{steel/mold},1}}\right|_{\underline{h}^{(k-1)}_{\text{steel/mold}}} & \cdots & \left.\frac{\partial Q_w^{\text{FEM}}}{\partial h_{\text{steel/mold},N_{\text{coef}}}}\right|_{\underline{h}^{(k-1)}_{\text{steel/mold}}} \end{bmatrix} \quad [22]$$

$$\underline{b}^T = \begin{bmatrix} \left(T_1^M - {}^{(k-1)}T_1^{\text{FEM}}\right) & \cdots & \left(T_{N\text{th}}^M - {}^{(k-1)}T_{N\text{th}}^{\text{FEM}}\right) \\ \left(Q_w^M - {}^{(k-1)}Q_w^{\text{FEM}}\right) \end{bmatrix} \quad [23]$$

In Appendix A, we discuss the calculation of the derivatives used in Eq. [22] (*sensitivity coefficients*).

(7) The linear system Eqn. [20] does not have a unique solution because there are more unknowns than equations (in general, $N_{\text{coef}} > N\text{th}+1$). Our purpose is to choose one of those infinite solutions, the one that best fits the physics of the problem.

(a) The first condition that we impose is that from all possible solutions, we choose the solution with the minimum norm; hence, we impose

$$\text{minimize } \frac{1}{2}\sum_{j=1}^{N_{\text{coef}}}\left(h^{(k)}_{\text{steel/mold,j}} - h^{(k-1)}_{\text{steel/mold,j}}\right)^2 = \text{minimize } \frac{1}{2}\,\|\,\underline{x}\,\|^2 \text{ under the constraint in Eq. [20]} \quad [24]$$

To improve the solution, we incorporate into the functional to be minimized our physical knowledge of the problem (*a priori information*).

(b) We know *a priori* that at the meniscus level, the heat flow between the steel and the mold has a local maximum; hence, the necessary condition is

$$\left.\frac{\partial \underline{h}_{\text{steel/mold}}}{\partial n}\right|_{\text{meniscus}} = 0 \quad [25]$$

where n is the mold axial direction.

In order to solve the minimization problem in Eq. [24] under the condition [25], we impose the necessary condition for a maximum:

$$\text{minimize } \left\|\frac{\partial \underline{h}_{\text{steel/mold}}}{\partial n}\right\|^2_{\text{meniscus}} \quad [26]$$

The interpolation functions adopted for the heat-transfer coefficient are piecewise constant; therefore, to calculate the derivatives in the Eq. [26], we use a finite difference operator: the matrix $\underline{L}^{\text{MAX}}$. Hence, we rewrite Eq. [26] as

$$\text{minimize } \frac{1}{2}\left\|\underline{L}^{\text{MAX}}\underline{h}^{(k)}_{\text{steel/mold}}\right\|^2 = \text{minimize } \frac{1}{2}\left\|\underline{L}^{\text{MAX}}(\underline{x} + \underline{h}^{(k-1)}_{\text{steel/mold}})\right\|^2 \quad [27]$$

However, we also have to impose the sufficient condition for a maximum. This condition can be

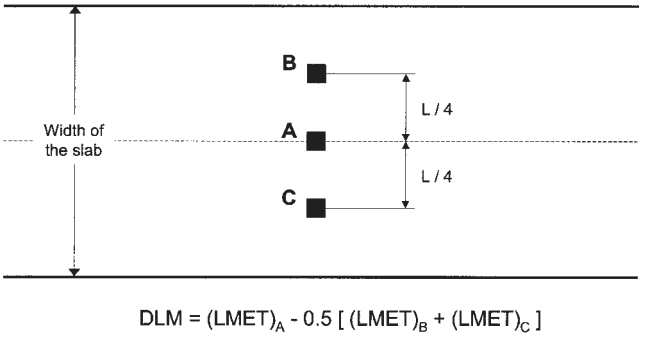

Fig. 9—Characterization of the solidification front shape.

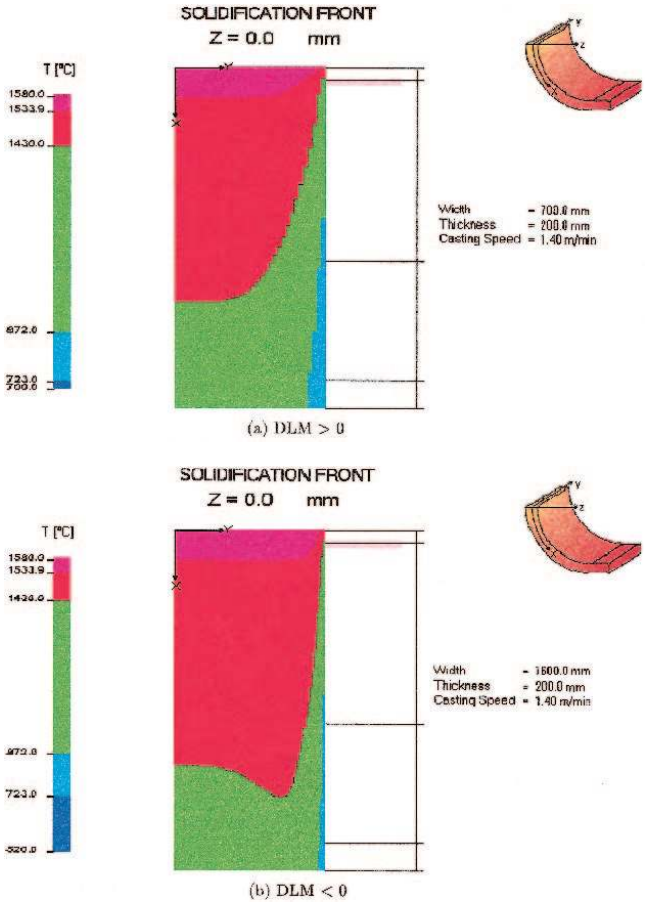

Fig. 10—(*a*) and (*b*) Typical solidification fronts.

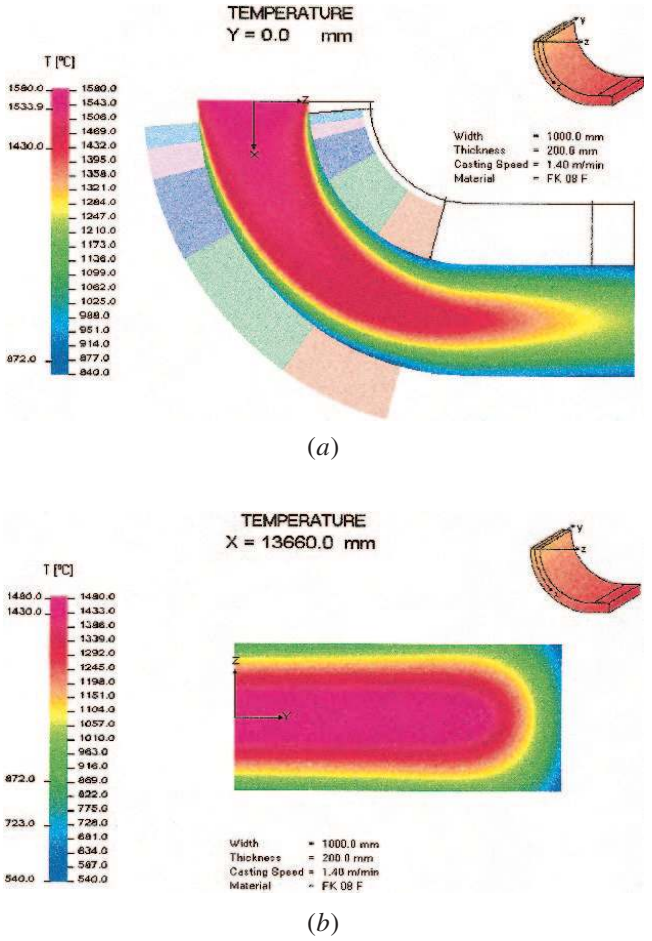

Fig. 11—Results for case 0: (*a*) temperature distribution in the central section and (*b*) temperature distribution in a transverse section at the exit of the water cooling zones.

written for every element containing the meniscus level as

$$g_i = (h_{\text{steel/mold},j} - h_{\text{steel/mold},i}) \leq 0 \qquad [28]$$

In Eq. [28] the i level is on the meniscus and the j level is immediately below. Hence, by adding the sufficient condition in Eq. [27], we obtain

$$\text{minimize } \frac{1}{2}\left\|\underline{L}^{\text{MAX}}(\underline{x} + \underline{h}^{(k-1)}_{\text{steel/mold}})\right\|^2 + \alpha^2 \sum_i \langle g_i \rangle \qquad [29]$$

In the preceding equation, α^2 is a penalty factor to be determined by numerical experimentation and $\langle \cdot \rangle$ are the Macauley brackets.

(c) We are seeking the heat-transfer coefficient distribution that approximates the actual heat flux distribution (unknown) and that matches the measured temperatures. We can assume it to be a smooth function; hence, we impose

$$\text{minimize } \left\|\nabla^2 \underline{h}_{\text{steel/mold}})\right\|^2 \qquad [30]$$

$$\text{minimize } \frac{1}{2}\left\|\underline{L}^{\text{SMT}}\, \underline{h}^{(k)}_{\text{steel/mold}}\right\|^2$$

$$= \text{minimize } \frac{1}{2}\left\|\underline{L}^{\text{SMT}}(\underline{x} + \underline{h}^{(k-1)}_{\text{steel/mold}})\right\|^2$$

$$\text{minimize } \frac{1}{2}\left(\|\underline{x}\|^2 + \left\|\underline{L}^{\text{MAX}}(\underline{x} + \underline{h}^{(k-1)}_{\text{steel/mold}})\right\|^2 \right.$$

$$\left. + \alpha^2 \sum_i \langle g_i \rangle + \left\|\underline{L}^{\text{SMT}}(\underline{x} + \underline{h}^{(k-1)}_{\text{steel/mold}})\right\|^2 \right)$$

under the constraint in Eq. [20]

$$\frac{-}{2}\left(\|\underline{x}\|^2 + \left\|\underline{L}^{\text{MAX}}(\underline{x} + \underline{h}^{(k-1)}_{\text{steel/mold}})\right\|^2 \right.$$

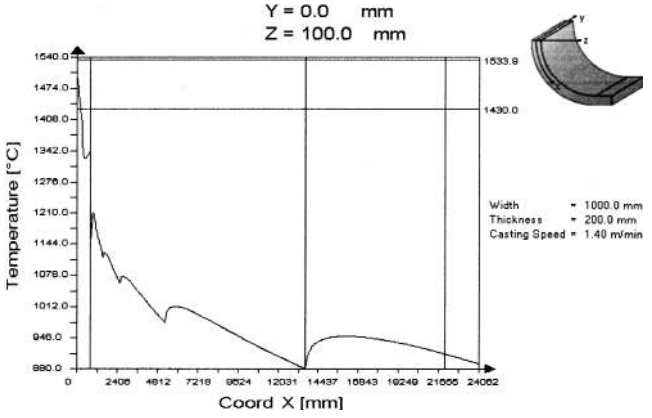

(*a*)

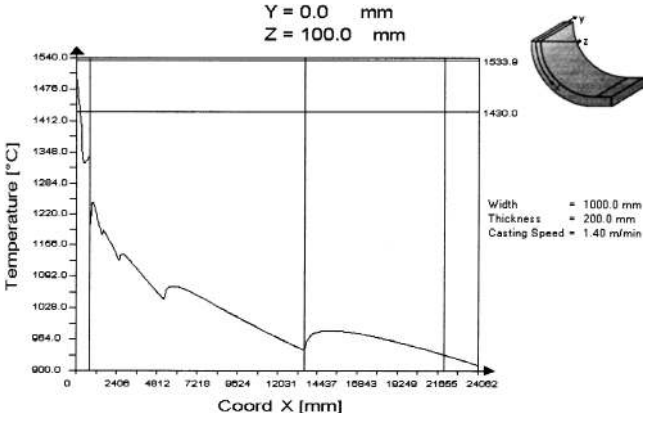

(*b*)

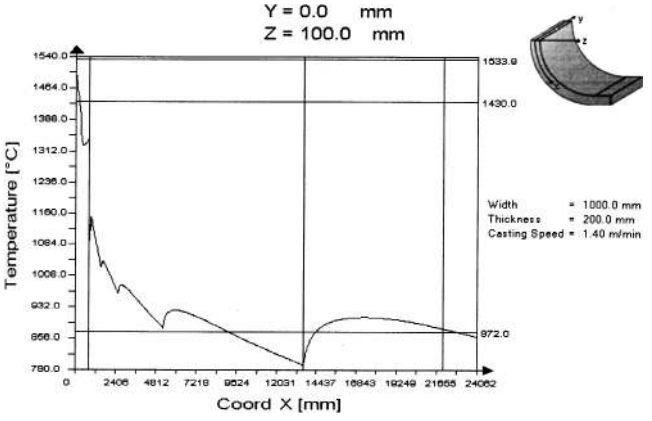

(*c*)

Fig. 12—Surface temperature distribution on the centerline of the upper face: (*a*) case 0, (*b*) case 10 (maximum surface temperature), and (*c*) case 9 (minimum surface temperature).

$$+\alpha^2\sum_i\langle g_i\rangle+\left\|\underline{L}^{\mathrm{SMT}}(\underline{x}+\underline{h}^{(k-1)}_{\mathrm{steel/mold}})\right\|^2\Big)+\underline{\lambda}^T(\underline{A}\,\underline{x}-\underline{b}) \quad [33]$$

The minimization of the preceding functional allows us to define the optimum vector $\underline{h}_{\mathrm{steel/mold}}$ corresponding to the adopted hypotheses and the set of initial values. Since there is a reduced number of thermocouples, the adopted set of initial values (*initial guess*) could condition the solution, especially in regions far from the thermocouples (Section IV–C).

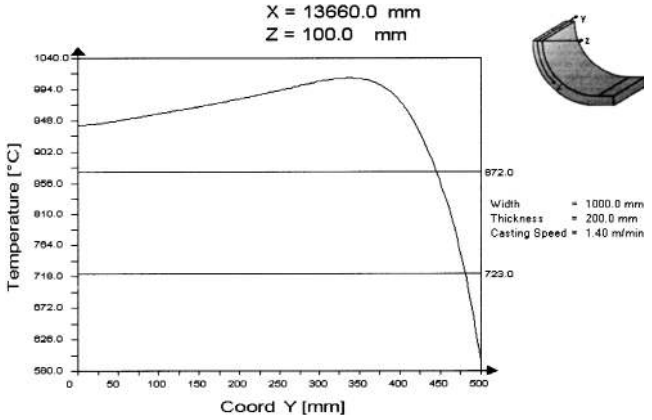

(*a*)

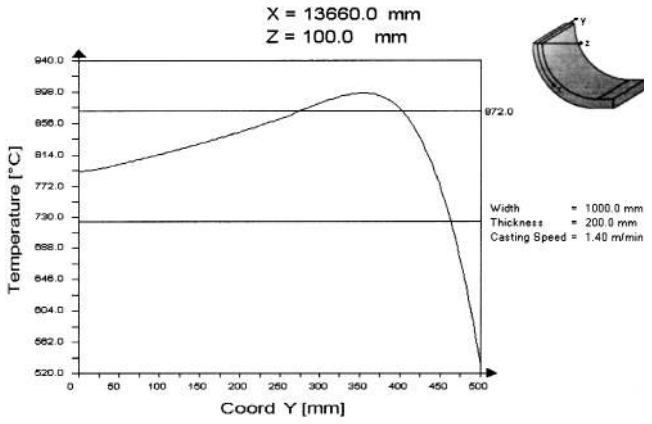

(*b*)

Fig. 13—Transversal surface temperature distributions at the exit of the water cooling zones: (*a*) case 10 (maximum surface temperature) and (*b*) case 9 (minimum surface temperature).

It is also convenient, according to our numerical experience, that when the external loop advances (iterations between CCAST-D and CCAST-1 in Figure 5), we decrease the relative magnitude of the *a priori* conditions, using a regularization parameter ε; hence, instead of Eq. [33], we use

$$\text{minimize}\ \frac{1}{2}\left(\|\underline{x}\|^2+\varepsilon\left(\left\|\underline{L}^{\mathrm{MAX}}(\underline{x}+\underline{h}^{(k-1)}_{\mathrm{steel/mold}})\right\|^2\right.\right. \quad [34]$$
$$\left.\left.+\alpha^2\sum_i\langle g_i\rangle+\left\|\underline{L}^{\mathrm{SMT}}(\underline{x}+\underline{h}^{(k-1)}_{\mathrm{steel/mold}})\right\|^2\right)\right)+\underline{\lambda}^T(\underline{A}\,\underline{x}-\underline{b})$$

$$\varepsilon=2^{-(\mathrm{ITER}-1)} \quad [35]$$

where ITER is the number of external iterations.

(8) $$\underline{h}^{(k)}_{\mathrm{steel/mold}}=\underline{h}^{(k-1)}_{\mathrm{steel/mold}}+\underline{x} \quad [36]$$

(9) Using the preceding equation in the mold finite-element model, we calculate ${}^{(k)}T_i^{\mathrm{FEM}}$ and ${}^{(k)}Q_w^{\mathrm{FEM}}$.

(10) If

$$\frac{\|T_i^M-{}^{(k)}T_i^{\mathrm{FEM}}\|^2}{\|T_i^M\|^2}+\frac{\|Q_w^M-{}^{(k)}Q_w^{\mathrm{FEM}}\|^2}{\|Q_w^M\|^2}\le\mathrm{TOL} \quad [37]$$

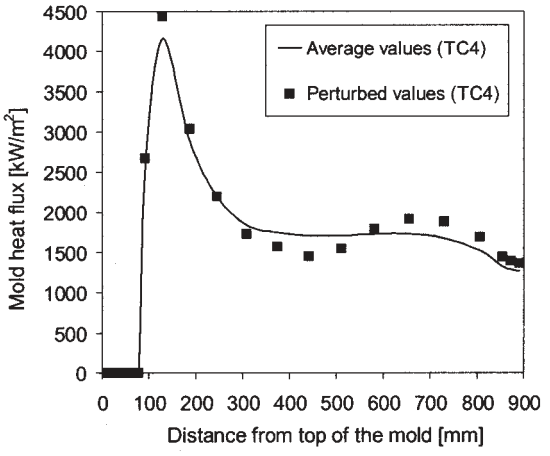

(a) Fixed side of the mold.

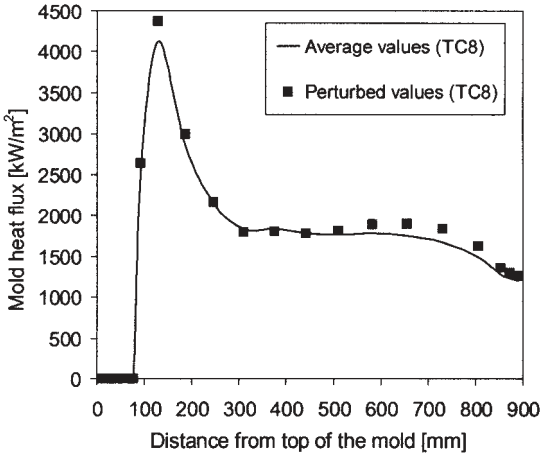

(b) Fixed side of the mold.

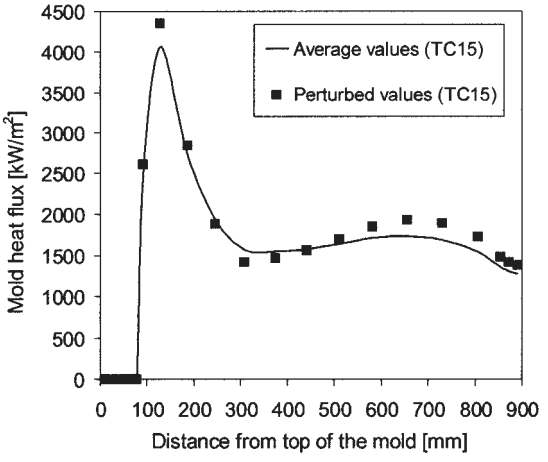

(c) Movable side of the mold.

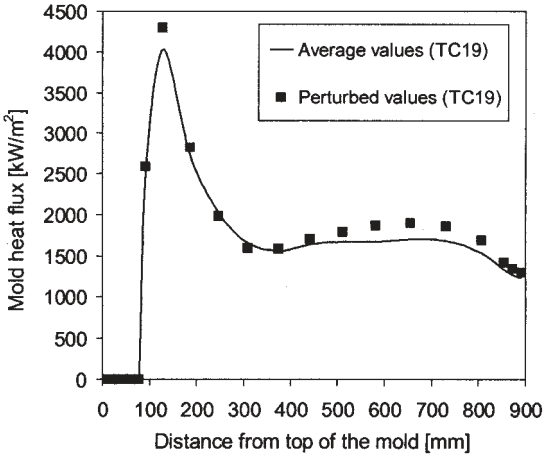

(d) Movable side of the mold.

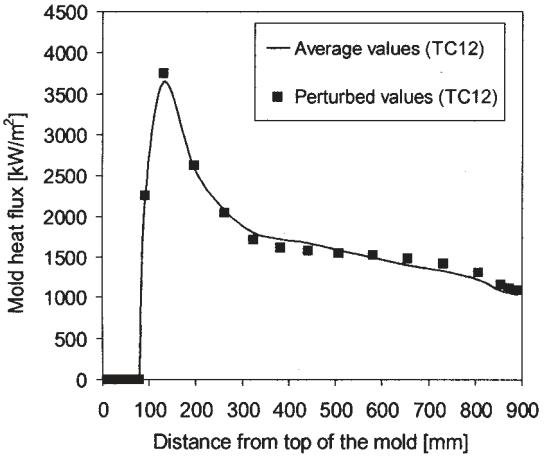

(e) Narrow side of the mold.

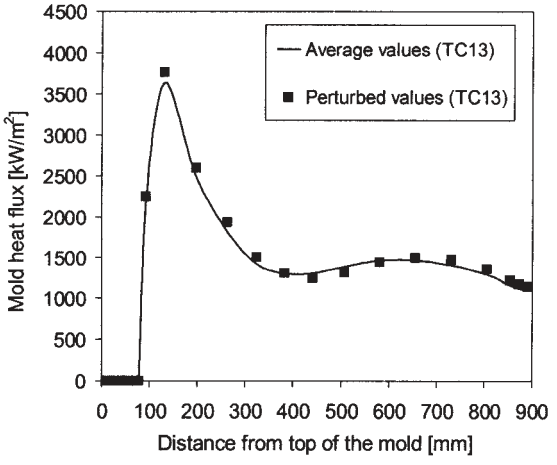

(f) Narrow side of the mold.

Fig. 14—(*a*) through (*f*) Stability test.

Table III. Average and Perturbed Set of Values Used in the Stability Test

Left Narrow Side	$\bar{x}$	s	$\bar{x}^e$	Right Narrow Side	$\bar{x}$	s	$\bar{x}^e$
G^M_{water} (L/min)	400.62	0.91	402.72	G^M_{water} (L/min)	400.13	1.72	399.38
$\Delta T^M_{\text{water}}$ (°C)	9.65	0.17	9.70	$\Delta T^M_{\text{water}}$ (°C)	10.08	0.14	10.25
TC1_Up (°C)	142.53	2.64	149.40	TC12_Up (°C)	174.54	2.81	170.98
TC1_Lo (°C)	134.79	3.53	128.84	TC12_Lo (°C)	146.89	3.14	141.82
TC2_Up (°C)	158.15	2.39	162.42	TC13_Up (°C)	150.51	2.42	156.83
TC2_Lo (°C)	137.88	2.75	131.45	TC13_Lo (°C)	126.05	3.39	121.12
Fixed Side	$\bar{x}$	s	$\bar{x}^e$	Movable Side	$\bar{x}$	s	$\bar{x}^e$
G^M_{water} (L/min)	3204.66	14.06	3192.49	G^M_{water} (L/min)	3199.98	16.87	3234.77
$\Delta T^M_{\text{water}}$ (°C)	9.03	0.14	9.41	$\Delta T^M_{\text{water}}$ (°C)	8.62	0.16	8.98
TC3_Up (°C)	32.39	0.24	32.90	TC14_Up (°C)	33.75	0.22	33.51
TC3_Lo (°C)	32.41	0.23	32.39	TC14_Lo (°C)	33.37	0.22	33.65
TC4_Up (°C)	117.55	3.62	115.56	TC15_Up (°C)	122.47	2.40	117.46
TC4_Lo (°C)	95.45	4.81	87.07	TC15_Lo (°C)	115.93	1.78	117.25
TC5_Up (°C)	124.62	2.33	125.70	TC16_Up (°C)	133.68	1.51	136.68
TC5_Lo (°C)	95.17	1.41	93.43	TC16_Lo (°C)	123.54	1.16	120.31
TC6_Up (°C)	124.22	2.36	118.98	TC17_Up (°C)	133.24	1.62	129.44
TC6_Lo (°C)	98.65	1.15	97.13	TC17_Lo (°C)	123.45	4.69	124.65
TC7_Up (°C)	125.59	2.59	126.59	TC18_Up (°C)	131.29	1.90	126.94
TC7_Lo (°C)	105.49	1.61	101.49	TC18_Lo (°C)	113.24	7.30	134.66
TC8_Up (°C)	121.11	2.80	121.00	TC19_Up (°C)	133.91	1.44	131.56
TC8_Lo (°C)	102.00	2.20	103.01	TC19_Lo (°C)	125.66	4.20	132.55
TC9_Up (°C)	124.44	2.48	125.37	TC20_Up (°C)	129.15	1.30	129.01
TC9_Lo (°C)	97.30	1.03	99.18	TC20_Lo (°C)	123.11	1.48	121.97
TC10_Up (°C)	129.05	3.05	131.12	TC21_Up (°C)	125.93	2.78	122.53
TC10_Lo (°C)	96.16	3.53	90.94	TC21_Lo (°C)	114.77	4.18	105.90
TC11_Up (°C)	34.58	0.31	34.92	TC22_Up (°C)	32.63	0.25	32.98
TC11_Lo (°C)	32.44	0.21	32.26	TC22_Lo (°C)	34.43	1.44	37.20

then the loop started at (1) has **CONVERGED**; if not **GO TO 4** (*TOL* is to be defined by the analyst).

IV. NUMERICAL EXPERIMENTATION

A. *Parametric Analyses of a Steel Slab's Continuous Casting Facility*

As a first example, we analyze, using only CCAST-D, a slab's continuous casting installation. In this first analysis, we use for the steel/mold heat exchange, the Savage–Pritchard empirical equation :

$$q_{\text{steel/mold}} = A - B\sqrt{\frac{z}{v}} \qquad [38]$$

For the present analysis we use,

$$A = 2680 \text{ W/m}^2 \text{ and } B = 335 \text{ W/m}^2 \text{ s}^{1/2}$$

Also,

z: distance to the meniscus (m), and
v: casting speed (m/s).

In this first set of analyses, we use the heat flows given by Eq. [38] in spite of our knowledge of the nonphysical results that it produces at the mold exit: cancellation and even inversion of the heat flow. We will improve the results, in the following analyses, using our inverse analysis with the information provided by the mold thermocouples.

In Figure 7, we show the different cooling zones downstream the mold exit, and in Figure 8, we indicate the water cooling arrangement used in each zone. For each of those zones, we use, for the heat exchange between the cooling water and the solidifying steel shell, a convection type heat-transfer model that takes into account the radiative and convective phenomena. In this model, the equivalent heat-transfer coefficient is

$$h_{\text{steel/water}} = \varepsilon\kappa \frac{[(T_{\text{slab}})^4 - (T_e)^4]}{(T_{\text{slab}} - T_{\text{water}})} + h_{\text{conv}} \qquad [39]$$

in Eq. [39], ε is the slab's emissivity coefficient (usually between 0.8 and 0.9), κ is the Boltzmann constant, T_{slab} is the slab's surface temperature, T_e is the external radiation temperature (between 60 °*C* and 80 °*C*), and T_{water} is the temperature of the cooling water.

It is important to notice that the term h_{conv} incorporates into a simplified convection model a number of different heat exchange phenomena:[22]

(1) heat exchange between the slabs and the guiding rolls,
(2) heat exchange between the slabs and the pool of water on its upper surface,
(3) heat exchange between the slabs and the water that flows under the rolls,
(4) heat exchange between the slabs and the cooling water impinging its surfaces.

For some analyses (*e.g.*, the fatigue of the solidified shell), it is of interest to model in detail the above phe-

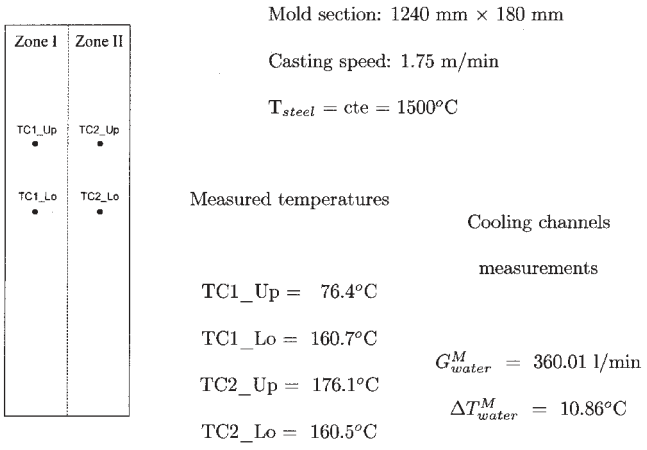

Fig. 15—Thermocouple distribution on the narrow plate of the instrumented slabs mold.

nomena.[23] However, for our purposes, the detailed analysis is not required and therefore we will lump all those effects into the coefficient h_{conv} that we calculate using[24]

$$h_{\text{conv}} = \frac{a\,(q_w)^b\,(1 - cT_w)}{\alpha} \qquad [40]$$

The preceding equation is an empirical formula in which we use the following units:

$$[h_{\text{conv}}] = \frac{\text{W}}{\text{m}^2\,^\circ\text{C}}$$

$$[q_w]\text{: water specific flow rate} = \frac{l}{\text{m}^2\,\text{s}}$$

$$[T_w] = ^\circ\text{C}$$

and the corresponding constants are[24]

$$a = 1570$$

$$b = 0.55$$

$$c = 0.0075$$

$$\alpha = 4$$

In order to investigate the sensitivity of the model results to the different operational parameters and model constants, we have analyzed the different combinations shown in Table I.

In Figure 10, in order to illustrate the significance of Dlm we present two results, one with Dlm > 0 and the other with Dlm < 0.

Some comments on the model results are provided as follows.

1. In Figure 11, we present the results for case 0, which are going to be used as a basis for the forthcoming comparisons.
2. For slabs of constant thickness (200 mm), the maximum metallurgical length corresponds to the maximum casting speed, while the minimum metallurgical length corresponds to the minimum casting speed. Hence, from all the parameters considered, the casting speed is the one with the most important effect on the metallurgical length. As we can also see (case 4), the slab thickness has an important effect on the metallurgical length.
3. In Figure 12, we present the surface temperature distribution on the centerline of the upper face for cases 0 (base case), 10 (maximum $Ts_{\max}$), and 9 (minimum $Ts_{\max}$). To illustrate the temperature distribution across the slab's width, in Figure 13, we graph the results for the temperature distribution on the slab's upper face, at the exit of the water cooling zone, for cases 10 and 9. It is evident from the analyzed cases that Tsmax is strongly influenced by the casting speed and by the water distribution inside each cooling zone.
4. The factors that influence the nonflatness of the solidification front, as measured by *Dlm*, are the slab's width (major influence), the slab's thickness, and the casting speed.

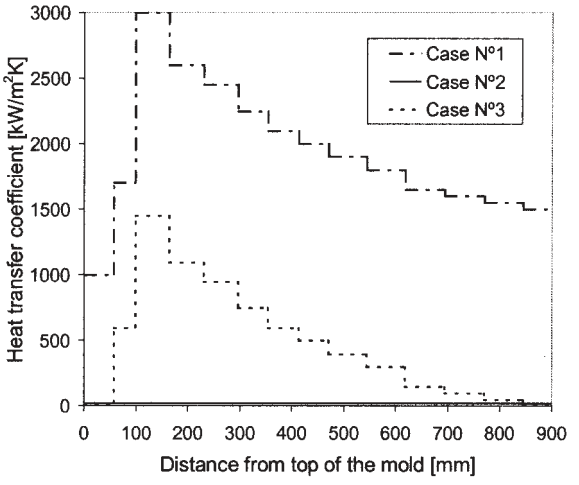

(a) Zone I

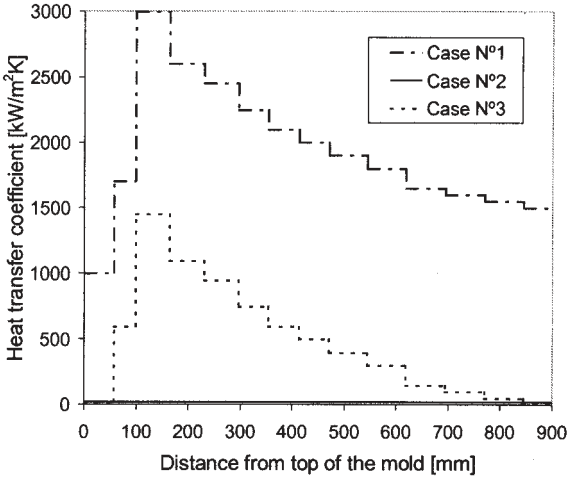

(b) Zone II

Fig. 16—(*a*) and (*b*) Three sets of initial values for the narrow plate analysis.

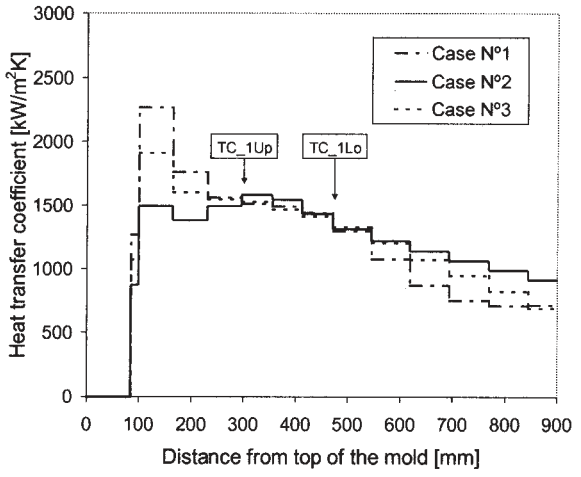

(a) Zone I

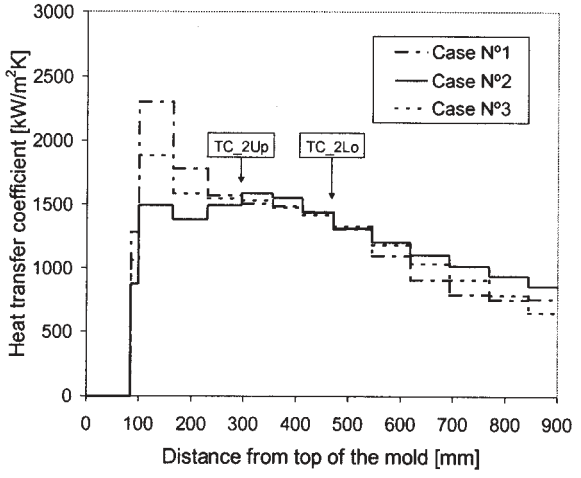

(b) Zone II

Fig. 17—(*a*) and (*b*) Results for $h_{\text{steel/mold}}$ obtained using the three sets of initial values.

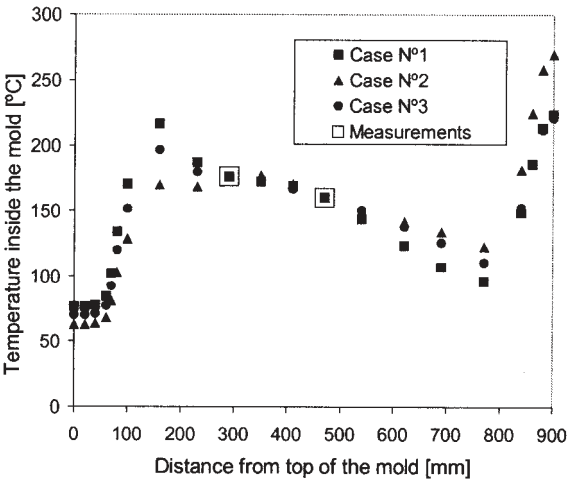

(a) Vertical line (TC1_Up - TC1_Lo)

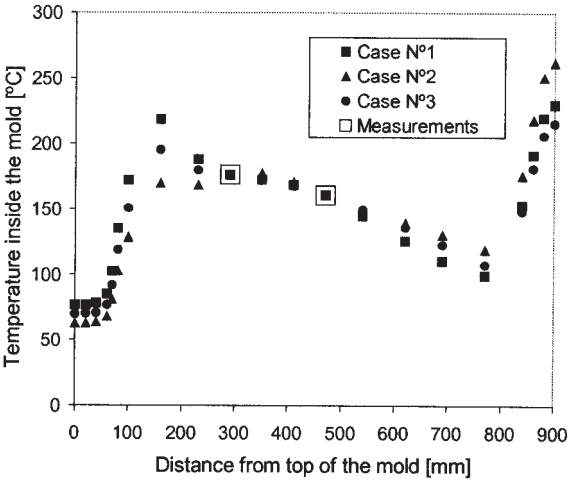

(b) Vertical line (TC2_Up - TC2_Lo)

B. *Stability Test*

In this subsection, we test the stability of the solutions provided by the CCAST system; for this purpose, we consider a set of thermocouple indications obtained during a period of time in which the setup of the operational variables was stationary. For each thermocouple, we consider its average indication and its standard deviation and then we run two analyses.

1. Using the average indication for each thermocouple.
2. Using a modified set of values: each thermocouple indication was modified using a random error proportional to its standard deviation:

$$T_i^{\varepsilon} = T_i^{\text{average}} + 3\varepsilon s_i$$

$$-1 \leq \varepsilon \leq 1 \text{ random variable}$$

s_i: standard deviation of the set of thermocouple indications for T_i

Also,

$$G_{\text{water}}^{\varepsilon} = G_{\text{water}}^{\text{average}} + 3\,\varepsilon s_{GW}$$

$$\Delta T_{\text{water}}^{\varepsilon} = \Delta T_{\text{water}}^{\text{average}} + 3\varepsilon s_{TW}$$

In Figure 14, we compare the results of both analyses for two thermocouple lines, and in Table III, we present the set of values used to run them. It can be observed that the results corresponding to the average and perturbed set of values are almost coincident; therefore, we can assess that the developed algorithm (CCAST-D + CCAST-I) provides very stable results.

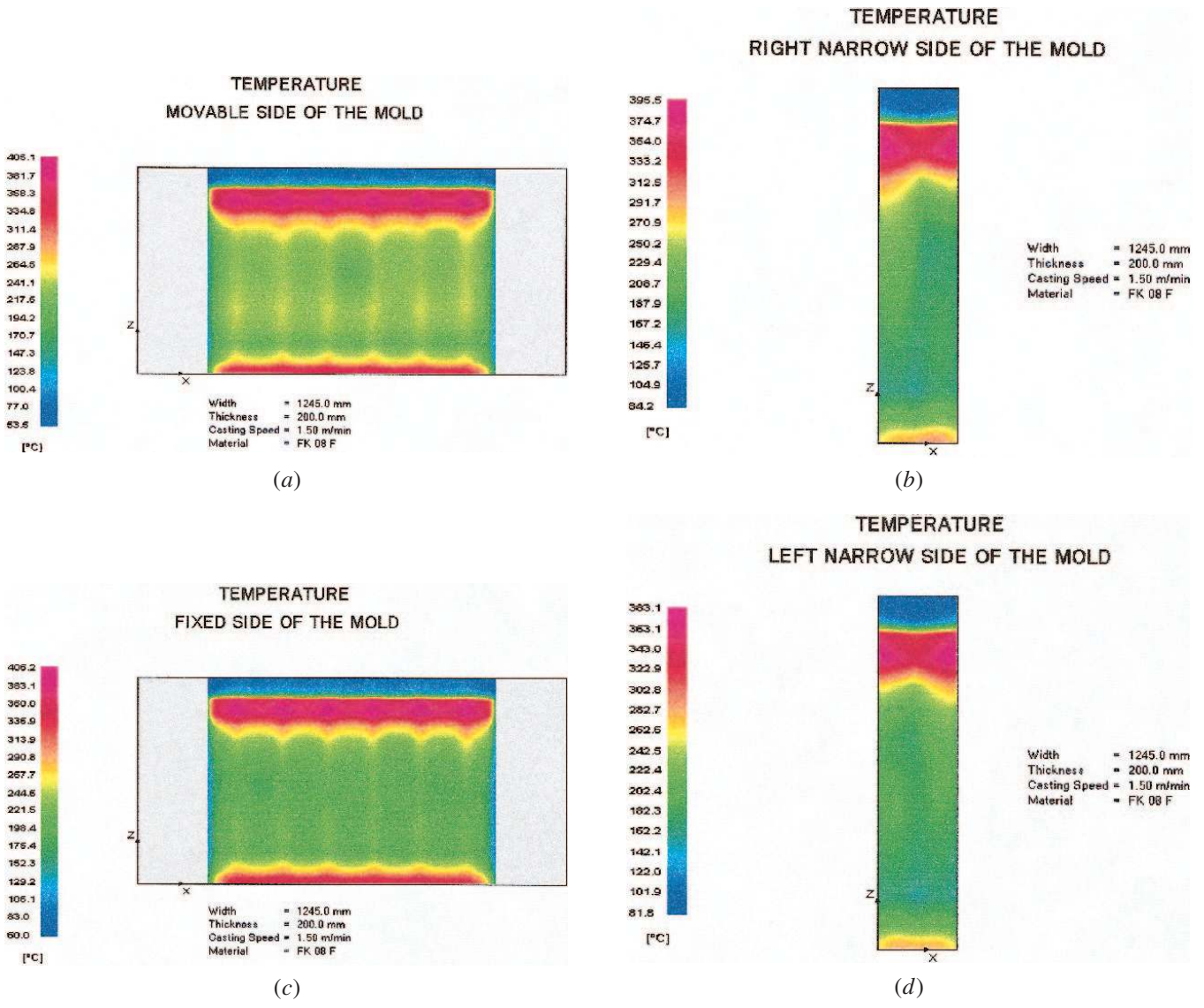

Fig. 19—Temperature maps predicted by CCAST for the mold plate hot faces: (*a*) movable side of the mold, (*b*) right narrow side of the mold, (*c*) fixed side of the mold, and (*d*) left narrow side of the mold.

C. *Effect of the Initial Values*

As we discussed in Section III of this article, the set of initial values that we use to start the inverse analysis (*initial guess*) may have an important influence on the calculation results; if this is the case, the calculation procedure looses reliability. In this numerical example, we analyze the influence of this *initial guess*.

For this purpose, we analyze, using CCAST, the narrow left plate of the instrumented slab's mold. We perform three analyses for the same set of thermocouple indications (Figure 15), but using three different sets of initial values for the steel/mold heat-transfer coefficients (Figure 16).

In Figure 17, we present the results of the three analyzed cases in terms of the predicted values of $h_{\text{steel/mold}}$. We observe that the three cases provide very close results in the thermocouples neighborhood and that the results present an acceptable spread in locations far from the thermocouples. However, as we show in Figure 18, the results obtained with the three sets of initial values are very similar when we represent them in terms of the mold predicted temperatures, except for the value of the peak temperature at the meniscus level.

D. *Analysis of an Industrial Case*

We use the CCAST system with the information provided by the thermocouples installed in a mold of SIDERAR continuous casting facility (San Nicolás, Argentina).

The thermocouple's data correspond to the average of the data acquired during a period of 28 minutes.

The casted steel chemical composition is indicated in Table IV.

In Figure 19, we show the temperature map predicted by the system for the hot faces of the mold plates. These maps do not show uniform temperature distributions due to the geometries of the water cooling channels and of the mold structure. Notice that the temperatures increase near the mold exit due to the lack of cooling water in this area of the analyzed mold.[25] In Figure 20, we represent the steel/mold heat fluxes predicted by our model.

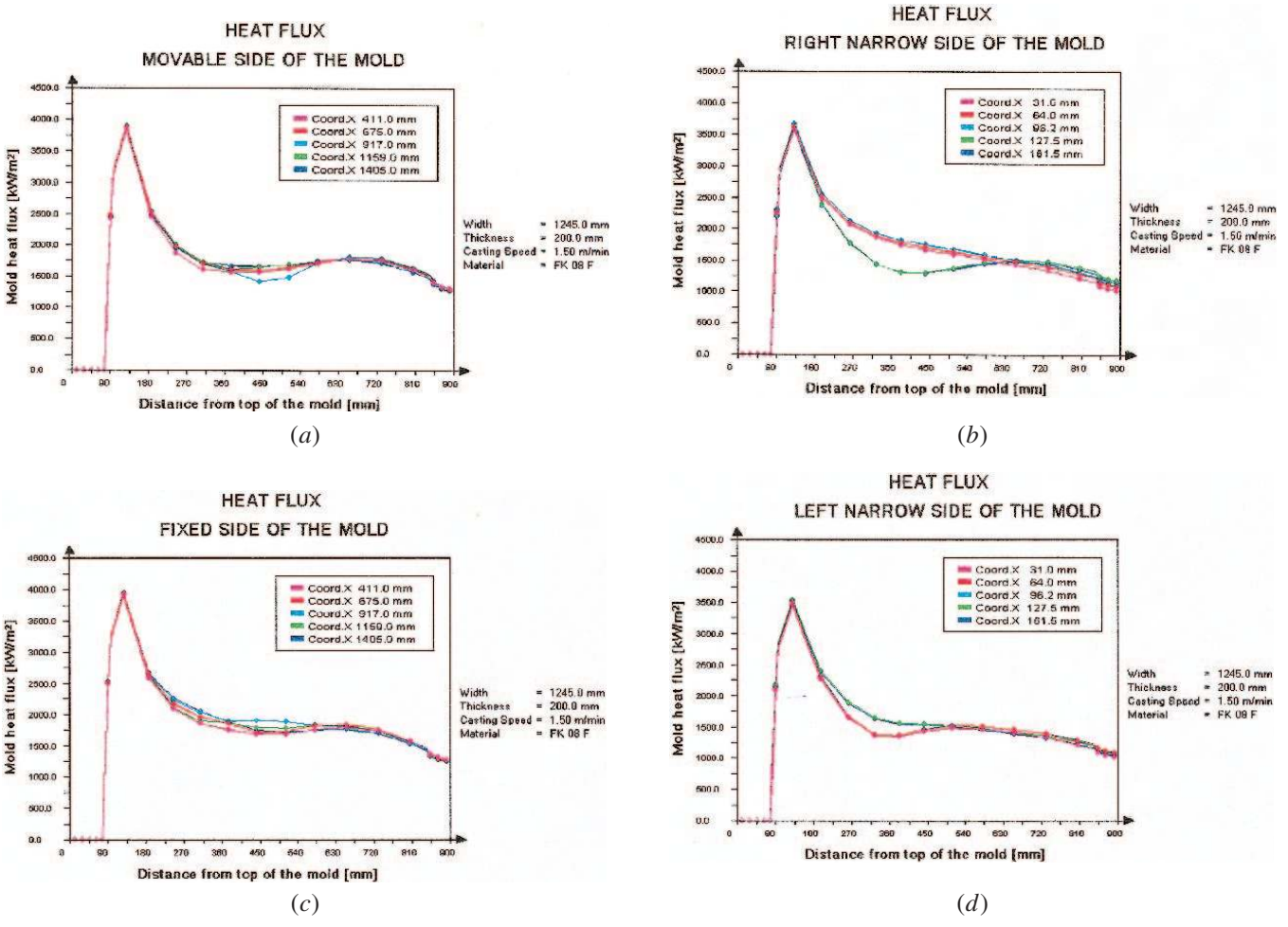

Fig. 20—Steel/mold heat fluxes predicted by CCAST: (*a*) movable side of the mold, (*b*) right narrow side of the mold, (*c*) fixed side of the mold, and (*d*) left narrow side of the mold.

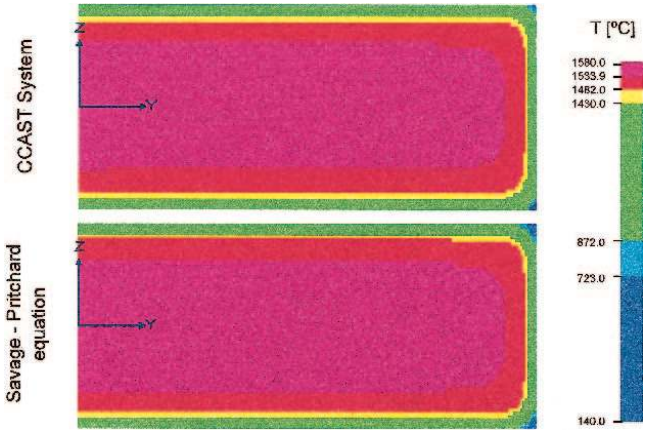

Fig. 21—Comparison between the results obtained using the inverse analysis procedure and the results obtained using the Savage–Pritchard equation.

In Figure 21, we compare the phase distribution results that were obtained, in a section located 800 mm downstream the meniscus, using

1. The complete CCAST system including the inverse analysis module.
2. CCAST-D with the steel/mold heat fluxes provided by the Savage–Pritchard equation adjusted to match the total heat extraction measured in the actual mold.

In Figure 22, to appreciate the difference between both approaches, we present a detailed comparison of the corner areas. The difference in these areas, at the mold exit, is as large as 300 °C; this result indicates that the Savage–Pritchard equation does not provide a good approximation in those areas where the gap is larger. Similar results have been reported in Reference 26.

V. CONCLUSIONS

In the present article, we reported the development of a computational simulation system for modeling the solidification process in a continuous casting facility for steel slabs. The system couples a module for solving the direct problem: the calculation of temperatures in the steel strand, with an inverse analysis module that we developed for evaluating the steel/mold heat fluxes from the information provided by thermocouples installed in the continuous casting mold copper plates.

In order to cope with the nonuniqueness of the inverse analysis, we incorporated to it *a priori* information that

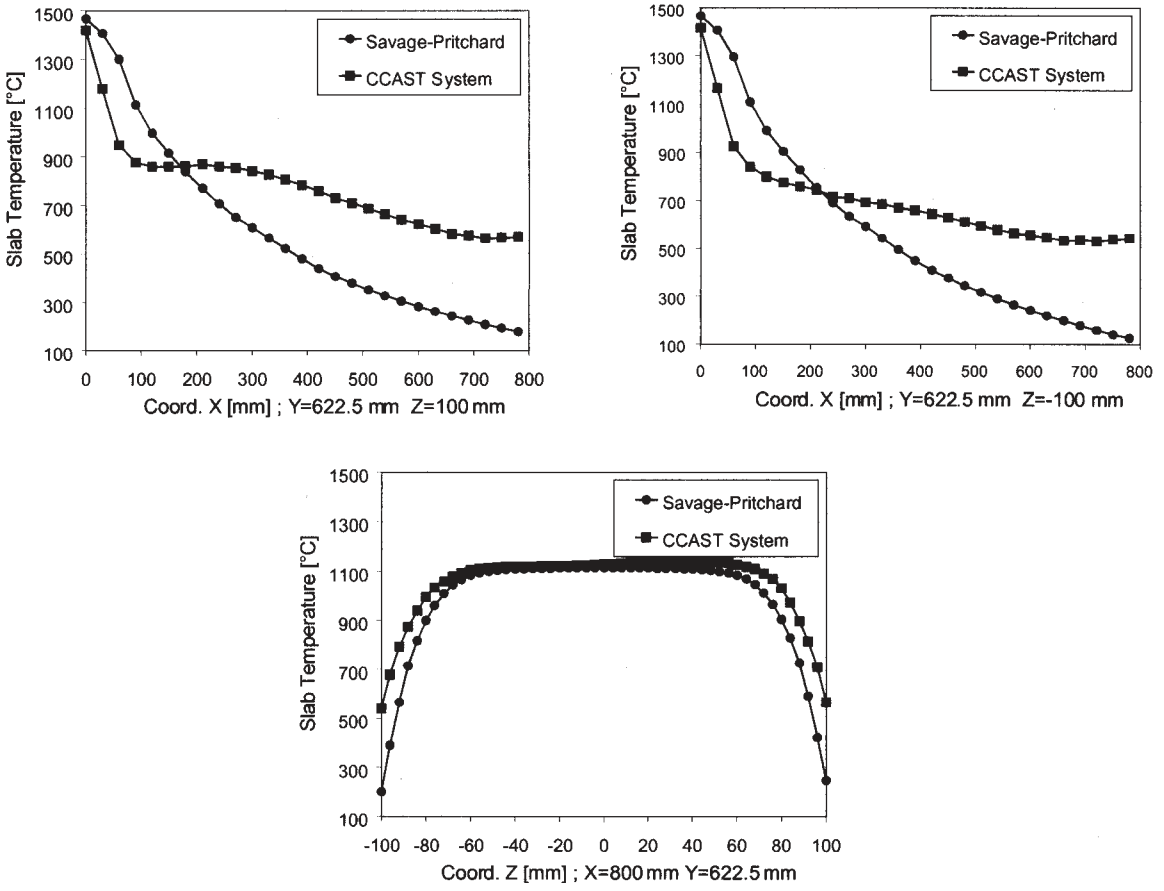

Fig. 22—Detail of the slab corner areas.

we have on the solution, based on the consideration of the problem physics.

We analyzed the stability of the system predictions and the influence of the first trial that we use to start the evaluation procedure. Finally, an industrial case was analyzed.

We can conclude, from the results of the analyzed cases, that the developed modeling system provides reliable engineering information for the analysis of actual industrial facilities.

At the present moment, the CCAST system is being used for analyzing the effect of different operational parameters and different casting powders on the thermal map of the continuous casted slabs. These thermal maps constitute a fundamental information to evaluate the slabs quality.

We are coupling the CCAST system to a finite-element program developed for calculating the thermal stresses that are developed in the steel strand.

ACKNOWLEDGMENT

We acknowledge the financial support and the information provided by SIDERAR (San Nicolás, Argentina).

APPENDIX
SENSITIVITY COEFFICIENTS

In this Appendix, we discuss the calculation of the sensitivity coefficients used for the inverse analysis in Eq. [22]: $\frac{\partial \underline{T}_{\text{mold}}}{\partial h_{\text{steel/mold},j}}$ and $\frac{\partial Q_w}{\partial h_{\text{steel/mold},j}}$

For the steady-state thermal problem in the mold, we have

$$\left[\underline{K}^k_{\text{mold}} + \underline{K}^c_{\text{water}} + \sum_{k=1}^{N_{\text{coef}}} h_{\text{steel/mold},\,k}\,\underline{K}^c_{\text{steel},\,k}\right]\underline{T}_{\text{mold}} = \underline{K}^c_{\text{water}}\underline{T}_{\text{water}} + \left[\sum_{k=1}^{N_{\text{coef}}} h_{\text{steel/mold},\,k}\,\underline{K}^c_{\text{steel},\,k}\right]\underline{T}_{\text{steel}} \quad [41]$$

Hence, we can obtain $\frac{\partial \underline{T}_{\text{mold}}}{\partial h_{\text{steel/mold},j}}$ from

$$\left[\underline{K}^k_{\text{mold}} + \underline{K}^c_{\text{water}} + \sum_{k=1}^{N_{\text{coef}}} h_{\text{steel/mold},\,k}\,\underline{K}^c_{\text{steel},\,k}\right]\frac{\partial \underline{T}_{\text{mold}}}{\partial h_{\text{steel/mold},j}} = \left[\sum_{k=1}^{N_{\text{coef}}} \delta_{j,k}\,\underline{K}^c_{\text{steel},\,k}\right](\underline{T}_{\text{steel}} - \underline{T}_{\text{mold}}) \quad [42]$$

In Eq. [42],

$$\underline{K}^{k}_{\text{mold}} = \int_{V_{\text{mold}}} \underline{B}^{T} k_{\text{mold}} \underline{B}\, dV \qquad [43a]$$

$$\underline{K}^{c}_{\text{water}} = \int_{S_{\text{water}}} h_{\text{water}} \underline{H}^{T}_{S} \underline{H}_{S}\, dS \qquad [43b]$$

$$\underline{K}^{c}_{\text{steel},k} = \int_{S_{\text{steel}}} N_{k} \underline{H}^{T}_{S} \underline{H}_{S}\, dS \qquad [43c]$$

where N_k are the piecewise constant interpolation functions used to discretize the heat-transfer coefficient function.

Also, from Eq. [13a], we obtain

$$\frac{\partial \underline{Q}_{w}}{\partial h_{\text{steel/mold},j}} = \int_{S_{\text{water}}} h_{\text{water}} \underline{H}_{S} \frac{\partial \underline{T}_{\text{mold}}}{\partial h_{\text{steel/mold},j}} dS \qquad [44]$$

REFERENCES

1. M.M. Wolf: *The Making, Shaping and Treating of Steel* Ironmaking Volume, 11th ed., AISE Steel Foundation, in press.
2. B. Lally, LT. Eiegler, and H. Henein: *Metall. Trans. B*, 1991, vol. 22B, pp. 641-48.
3. B. Lally, L.T. Biegler, and H. Henein: *Metall. Trans. B*, 1991, vol. 22B, pp. 649-59.
4. E.N. Dvorkin: *IACM-Expressions*, 2001, Jan., No. 10.
5. M.R. Ridolfi and B.G. Thomas: *La Rev. Métall.–CIT*, 1994, Apr., pp. 609-20.
6. J.E. Kelly, K.P. Michalek, T.G. O'Connor, B.G. Thomas, and J.A. Dantzig: *Metall. Trans. A*, 1988, vol. 19A, pp. 2589-602.
7. J. Savage and W.H. Pritchard: *J. Iron Steel Inst.*, 1954, Nov., pp. 29-77.
8. J.E. Lait, J.K. Brimacombe, and F. Weinberg: *Ironmaking and Steelmaking (Q.)* 1974, vol. 2, pp. 90-97.
9. K. Morgan, R.W. Lewis, and O.C. Zienkiewicz: *Int. J. Num. Methods Eng.*, 1977, vol. 12, pp. 1191-95.
10. W.D. Rolph and K.J. Bathe: *Int. J. Num. Methods Eng.*, 1982, vol. 18, pp. 119-34.
11. K.K. Tamma and R.R. Namburu: *Int. J. Num. Methods Eng.*, 1990, vol. 30, pp. 803-20.
12. R. Song, G. Dhatt, and A. Ben Cheikh: *Int. J. Num. Methods Eng.*, 1990, vol. 30, pp. 579-99.
13. C.R. Swaminathan and V.R. Voller: *Metall. Trans. B*, 1992, vol. 23B, pp. 651-64.
14. L.A. Crivelli and S.R. Idelsohn: *Int. J. Num. Methods Eng.*, 1986, vol. 23, pp. 99-119.
15. M.A. Storti, L.A. Crivelli, and S.R. Idelsohn: *Int. J. Num. Methods Eng.*, 1987, vol. 24, pp. 375-92.
16. V.D. Fachinotti, A. Cardona, and A.E. Huespe: *Int. J. Num. Methods Eng.*, 1999, vol. 44, pp. 1863-84.
17. J. Miettinen: *Metall. Mater. Trans. B*, 1997, vol. 28B, pp. 281-95.
18. R.J. Bathe: *Finite Element Porcedures*, Prentice-Hall, Upper Saddle River, NJ, 1996.
19. H. Matthies and G. Strang: *Int. J. Num. Methods Eng.*, 1979, vol. 14, pp. 1613-26.
20. A.F. Mills: *Heat Transfer*, IRWIN, 1992.
21. D.G. Luenberger: *Linear Nonlinear Programming.*, Addison C Wesley, Reading, MA, 1984.
22. S. Louhenkilpi: *Scand. J. Metall.*, 1994, vol. 23, pp. 9-17.
23. S.G. Hibbins and J.K. Brimacombe: *Continuous Casting*, vol. 2, *Heat Flow, Solidification and Crack Formation*, ISS-AIME, Pittsburgh, PA, 1984, pp. 139-51.
24. J.K. Brimacombe, P.K. Agarawal, L.A. Baptista, S.G. Hibbins, and B. Prabhakar: *Proc. 69th Steelmaking Conf. Proc.*, ISS-AIME, Washington, DC, 1986, pp. 109-23.
25. I.V. Samarasekera and J.K. Brimacombe: *Proc. 3rd PTD Conf. on Application of Mathematical and Physical Models in the Iron and Steelmaking Industry*, ISS, Pittsburgh, PA, 1982, 283-95.
26. B.G. Thomas, G. Li, A. Moita, and D. Habing: *ISS Trans.*, 1998, pp. 125-43.